

## High-order-harmonic generation from solids: The contributions of the Bloch wave packets moving at the group and phase velocities

Tao-Yuan Du,<sup>1,2</sup> Xiao-Huan Huang,<sup>3,\*</sup> and Xue-Bin Bian<sup>1,†</sup>

<sup>1</sup>State Key Laboratory of Magnetic Resonance and Atomic and Molecular Physics, Wuhan Institute of Physics and Mathematics, Chinese Academy of Sciences, Wuhan 430071, China

<sup>2</sup>School of Physical Sciences, University of Chinese Academy of Sciences, Beijing 100049, China

<sup>3</sup>Hubei Key Laboratory of Pollutant Analysis and Reuse Technology, College of Chemistry and Chemical Engineering, Hubei Normal University, Huangshi 435002, China



(Received 18 July 2017; published 10 January 2018)

We study numerically the Bloch electron wave-packet dynamics in periodic potentials to simulate laser-solid interactions. We introduce an alternative perspective in the coordinate space combined with the motion of the Bloch electron wave packets moving at group and phase velocities under the laser fields. This model interprets the origins of the two contributions (intra- and interband transitions) in the high-order harmonic generation (HHG) processes by investigating the local and global behaviours of the wave packets. It also elucidates the underlying physical picture of the HHG intensity enhancement by means of carrier-envelope phase, chirp, and inhomogeneous fields. It provides a deep insight into the emission of high-order harmonics from solids. This model is instructive for experimental measurements and provides an alternative avenue to distinguish mechanisms of the HHG from solids in different laser fields.

DOI: [10.1103/PhysRevA.97.013403](https://doi.org/10.1103/PhysRevA.97.013403)

### I. INTRODUCTION

The techniques in attosecond sciences, traditionally applied to atoms and molecules in the gas phase [1,2], have been extended to the bulk solids recently [3–20]. A crucial difference between bulk solids and gas targets is the localization of the initial electron wave packet, which is spatially confined in isolated atoms and molecules but can be delocalized in solids. The effect of electron distribution on wave-packet dynamics of laser-solid interaction remains elusive. A semiclassical model [21] is proposed, which is in analogy with the three-step model for high-order harmonics generated from the atomic and molecular systems in the coordinate space [22,23] by requiring that the electron-hole pair have the same displacement, i.e.,  $x_c - x_v = 0$ . Our theoretical work also introduces a quasi-classical model [24,25] to investigate the electron dynamic processes under the laser fields in the wave-vector  $k$  space, based on the delocalization of the wave packet. However, the two models cannot reveal the origins of high-order harmonic generation (HHG) from the time-dependent evolution of the Bloch electron wave packet between neighboring atomic sites in the coordinate space. To understand the process of the HHG from solids intuitively, a further picture in the coordinate space is required. Theoretically, the contributions to HHG in crystal solids have been divided into intra- and interband transitions [26–28]. The intra- and interband models describe particlelike electron and hole moving in the  $\epsilon$ - $k$  (energy-wave-vector) space. However, the key role of these two contributions remains intensively debated [28,29]. In the quantum picture,

the dynamics of electrons are described by Bloch waves. In this work, we explore the intra- and interband transitions by investigating the Bloch wave-packet oscillations in the  $x$ - $t$  (coordinate-time) space.

Our work provides insight into the process of HHG in crystal solids by focusing on the two underlying nonlinear currents, which are caused by the motion of the Bloch electron wave packets moving at group and phase velocities in the coordinate space, respectively. This model reveals that the two nonlinear currents ( $j_{\text{group}}$  and  $j_{\text{phase}}$ ) correspond to the global and local oscillation motion of the wave packet in the coordinate space, respectively. Pictures in  $k$  space show a good agreement with those in the coordinate space. Atomic units are used throughout unless stated otherwise.

### II. THEORETICAL APPROACH

During the laser fields interacting with solids, Bloch electrons in the valence band have probabilities to tunnel to conduction bands, i.e., Zener tunneling [30–32]. But the tunneling probabilities exponentially decay with the increase of energy gap. Only a small portion of electrons, which are populated on top of the valence band near the wave vector  $k = 0$  with minimal band gap, can tunnel to conduction bands with the laser parameters used in the current work. So we choose an initial wave function in the valence band which is superposed by the  $\Delta k$  Bloch eigenstates near  $k_0 = 0$  [33]. We can regard the initial Bloch wave packet as a quasiparticle. Based on the assumption, the quasiparticle wave packet can be written as [34,35]

$$\psi_k^n(x, t) = e^{i[kx - \frac{\epsilon_n(k)}{\hbar}t]} u_k^n(x), \quad (1)$$

where  $u_k^n(x)$  is a function with period in the lattice constant  $a_0$  and  $\epsilon_n(k)$  represents eigenvalue of the energy. The Bloch wave

\*xhuang@hbnu.edu.cn

†xuebin.bian@wipm.ac.cn

packet at a given wave vector  $k_0$  in band  $n$  can be superposed by the wave functions of  $\Delta k$  near the  $k_0$  in the same band. It can be represented as

$$\Psi_{k_0}^n(x, t) = \frac{1}{\Delta k} \int_{k_0 - \frac{\Delta k}{2}}^{k_0 + \frac{\Delta k}{2}} u_k^n(x) e^{i[kx - \frac{\epsilon_n(k)}{\hbar}t]} dk. \quad (2)$$

The Taylor expansion of eigenenergy  $\epsilon_n(k)$  near  $k_0$  can be expressed as

$$\epsilon_n(k) = \epsilon_n(k_0) + [\nabla_k \epsilon_n(k)]_{k_0} \delta k + \dots, \quad (3)$$

and the amplitude modulation factor  $u_k^n(x)$  changes slowly with  $k$ . So the Eq. (2) can be rewritten as

$$\begin{aligned} \Psi_{k_0}^n(x, t) &\approx \frac{u_{k_0}^n(x)}{\Delta k} e^{i[k_0 x - \frac{\epsilon_n(k_0)}{\hbar}t]} \\ &\times \int_{-\frac{\Delta k}{2}}^{\frac{\Delta k}{2}} e^{i[\delta k(x - \frac{[\nabla_k \epsilon_n(k)]_{k_0}}{\hbar}t)]} d(\delta k), \end{aligned} \quad (4)$$

we finally come to

$$\begin{aligned} \Psi_{k_0}^n(x, t) &\approx \psi_{k_0}^n(x, t) \frac{\sin \frac{\Delta k}{2} \zeta}{\frac{\Delta k}{2} \zeta} \\ &= \psi_{k_0}^n(x, t) \Phi(x, t), \end{aligned} \quad (5)$$

where  $\zeta = x - \frac{1}{\hbar} (\frac{\partial \epsilon_n(k)}{\partial k})_{k_0} t$ . The wave function can be divided into two parts naturally. Electronic probability at atomic sites in coordinate space is defined by

$$|\Psi_{k_0}^n(x, t)|^2 = |\psi_{k_0}^n(x, t)|^2 |\Phi(x, t)|^2. \quad (6)$$

It implies that the electronic probability is the modulus square of the periodic lattices ( $|\psi_{k_0}^n(x, t)|^2$ ) modulated by the envelope ( $|\Phi(x, t)|^2$ ). The envelope involves the information of the energy bands.

We describe the light-solid interaction in one dimension, along the polarization direction of the laser fields. In the length-gauge treatment, the time-dependent Hamiltonian is written as

$$\hat{H}(t) = \hat{H}_0 + xE(t), \quad (7)$$

where  $\hat{H}_0 = \frac{\hat{p}^2}{2} + V(x)$ , and  $V(x)$  is a periodic lattice potential. In our calculations, we choose the Mathieu-type potential [19,33,36]. The specific form is  $V(x) = -V_0[1 + \cos(2\pi x/a_0)]$ , with  $V_0 = 0.37$  a.u. and lattice constant  $a_0 = 8$  a.u., respectively. The band gap and lattice constant mimic the structure of AlN with a 4.2 eV band gap.

The energy band structure and time-dependent Schrödinger equation (TDSE) can be solved by using Bloch states in the  $k$  space and  $B$  splines in the coordinate space, respectively. For details we refer readers to Refs. [37,38]. After obtaining the time-dependent wave function  $\Psi_{k_0}^n(x, t)$  at an arbitrary time, we can calculate the laser-induced currents by dividing it into two contributions according to Eq. (5). It can be written as

$$\begin{aligned} j_{\text{phase}}(t) &= \frac{i}{2} \sum_{s=1}^N \int_{x_s}^{x_{s+1}} \left[ \psi_{k_0}^{n*}(x, t) \frac{\partial}{\partial x} \psi_{k_0}^n(x, t) \right. \\ &\quad \left. - \psi_{k_0}^n(x, t) \frac{\partial}{\partial x} \psi_{k_0}^{n*}(x, t) \right] dx \end{aligned} \quad (8)$$

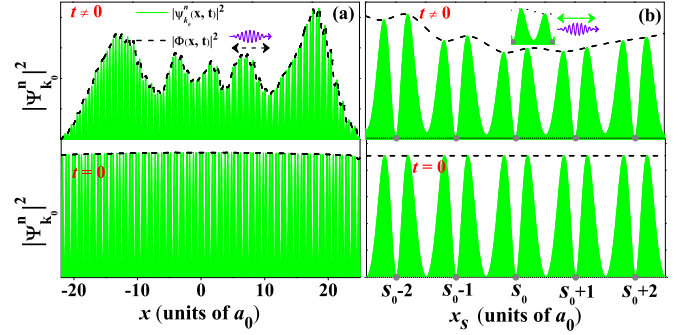


FIG. 1. Scheme of the time-dependent electron wave-packet evolution process for the HHG from periodic lattice crystal. The periodic atomic site is represented by the gray circles along the black dash line. The bottom of panel (a) depicts the initial wave packet with  $k_0 = 0$  at the top of the valence band ( $n = 1$ ), while the top of the panel (a) shows a snapshot of the time-dependent evolution of the electron wave packet driven by the laser fields. The periodic fine structure ( $|\psi_n^{k_0}(x, t)|^2$ ) and the envelope ( $|\Phi(x, t)|^2$ ) of the electron wave packet are shown by the green solid line and black dash line, respectively. Panel (b) presents a local amplification of the wave packet. Due to the electron excitation-recombination process under the laser fields, the oscillations of the electron wave packet between neighboring atomic sites, as shown in the inset of the panel (b), give rise to the emission of HHG. The two-way arrows and the wiggly lines denote the back and forth oscillation of the wave packet and the emission of HHG, respectively.

and

$$\begin{aligned} j_{\text{group}}(t) &= \frac{i}{2} \int \left[ \Phi^*(x, t) \frac{\partial}{\partial x} \Phi(x, t) \right. \\ &\quad \left. - \Phi(x, t) \frac{\partial}{\partial x} \Phi^*(x, t) \right] dx, \end{aligned} \quad (9)$$

where the  $N$  and  $x_s$  are the index of the lattice site and the coordinates of the periodic lattice, respectively. Equations (8) and (9) imply that the two nonlinear currents correspond to the Bloch wave packet moving at phase and group velocities in the laser fields, respectively. The current  $j_{\text{phase}}$  is caused by the electron polarization between each two neighboring lattice sites, which is shown in the inset of the top panel in the Fig. 1(b). Based on the physical picture and the Appendix, we combine the time-dependent electron population and energy band dispersion of the each band, the Eq. (9) can be reduced to [34,35]

$$j_{\text{group}}(t) = - \sum_{n=c,v} \int \rho_n \frac{\partial \epsilon_n}{\partial k} \Big|_{k=k_0+A(t)} dk, \quad (10)$$

where  $\rho_n$  and  $\frac{\partial \epsilon_n}{\partial k}$  represent the population and group velocity of the electron (hole) in the band  $n$ , respectively.  $A(t)$  is the vector potential of the laser fields. The HHG power spectrum is proportional to  $|j(\omega)|^2$ , the modulus square of Fourier transform of the time-dependent currents in Eqs. (8) and (10).

### III. RESULTS AND DISCUSSION

We study the time-dependent electron wave-packet evolution process during the laser-solid interaction. Figure 1(a)

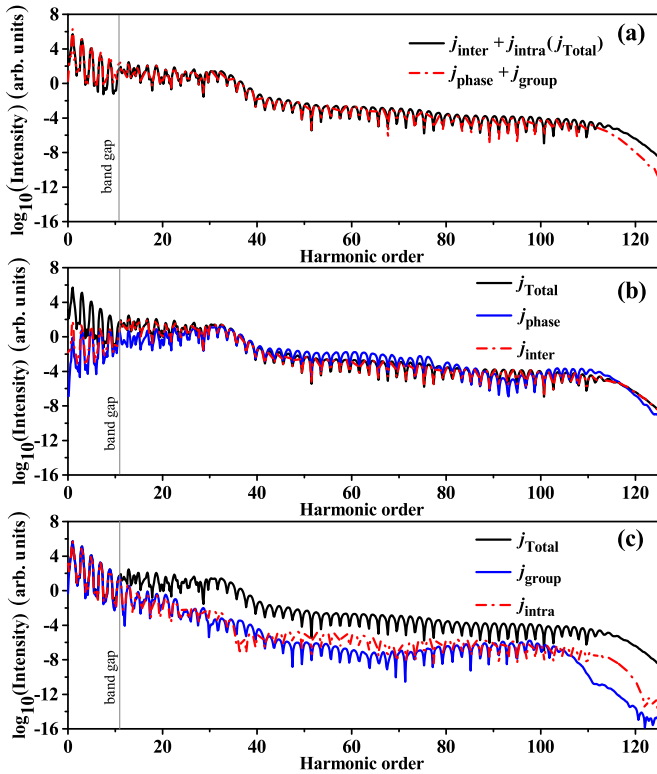


FIG. 2. Comparison of the current model and the previous models [21,37,38]. (a) Comparison of HHG obtained by  $j_{\text{phase}} + j_{\text{group}}$  and  $j_{\text{inter}} + j_{\text{intra}}$ . (b) Comparison of HHG obtained by  $j_{\text{phase}}$  and  $j_{\text{inter}}$ . (c) Comparison of HHG obtained by  $j_{\text{group}}$  and  $j_{\text{intra}}$ . The intensity, wavelength, and duration of the driving laser pulses are set to be  $0.87 \text{ TW/cm}^2$ ,  $3.2 \mu\text{m}$ , and eight optical cycles, respectively.

shows the full view of the electron wave-packet evolution in the fields. The wave-packet oscillations between the lattice sites are shown in the Fig. 1(b). Time-dependent envelope function (the black dash line) of the electron wave packet depicts the nonlinear current in Eqs. (9) and (10). The electron wave-packet amplitude difference between each two neighboring atomic sites in the time-dependent periodic fine structure, as shown in the inset of Fig. 1(b), describes the charge density polarization under the laser fields. The time-dependent polarization can be obtained by integrating the current in Eq. (8). It gives rise to the HHG. In summary, both the oscillations of the envelope function and periodic fine structure between each two lattice sites give rise to the HHG emissions.

### A. Validity of the model

The harmonic spectra generated by the two nonlinear currents are shown in Fig. 2. The total harmonic spectrum is depicted by the solid black line, which characterizes a rapid decay and double-plateau structure. One can find that the currents  $j_{\text{phase}}$  and  $j_{\text{group}}$  play key roles in the HHG process in the plateau and the below gap zones, as in Figs. 2(b) and 2(c), respectively. We also calculated  $j_{\text{inter}}$  and  $j_{\text{intra}}$ . The details can be found in Ref. [38]. Their contributions are also illustrated in Fig. 2. One may find that the roles between  $j_{\text{inter}}$  and  $j_{\text{phase}}$  are quite close, which dominate the HHG in the plateau. The roles

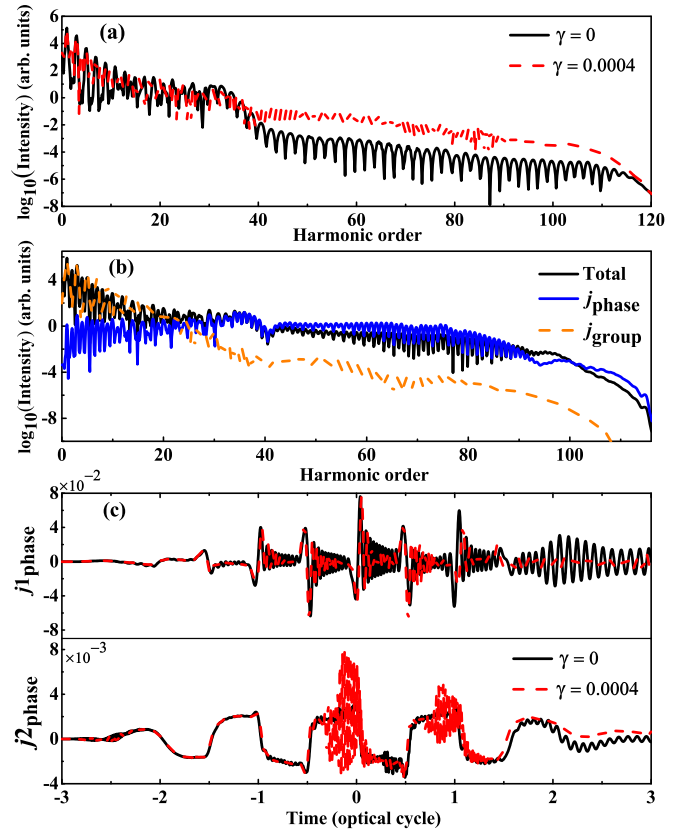


FIG. 3. (a) The yields enhancement of the HHG under the inhomogeneous fields with a nonhomogeneity parameter  $\gamma = 0.0004$  a.u. (b) The key contributions of the HHG spectrum under the inhomogeneous fields are displayed. (c) Comparison of the currents  $j_{\text{phase}}$  between homogeneous and inhomogeneous fields. The top and bottom of panel (c) show the currents ( $j_{1\text{phase}}$  and  $j_{2\text{phase}}$ ) contributing to the HHG spectra of the first and second plateau, respectively. The laser parameters are the same as those in Fig. 2.

between  $j_{\text{intra}}$  and  $j_{\text{group}}$  are also closely equal, which dominate in the lower-order harmonics.

To further compare the roles of  $j_{\text{inter}}$ ,  $j_{\text{phase}}$ ,  $j_{\text{intra}}$ , and  $j_{\text{group}}$ , we coherently add their contributions to the HHG shown in Fig. 2(a). One may find perfect agreements after considering the approximations in Eq. (5). The comparison of the current model and previous models reveals the physical picture of the currents  $j_{\text{group}}$  and  $j_{\text{phase}}$ , which correspond to the intraband Bloch oscillations and interband transition dynamics, respectively. The insight into the HHG process provides an intuitive understanding on the role of the dominant contribution in the laser fields with the wavelength ranging from midinfrared to Terahertz (THz) region.

### B. Contribution of wave packets on group and phase velocities

To further investigate the mechanisms of HHG, we reinterpret the intensity enhancement in the HHG process by regulating the laser parameters such as the spacial nonhomogeneity, carrier-envelope phase (CEP), and chirp.

We first perform an analysis of the HHG yield enhancement in solids under the nonhomogeneous (plasmon-enhanced) fields, as shown in Fig. 3. It has been reported theoretically [37]

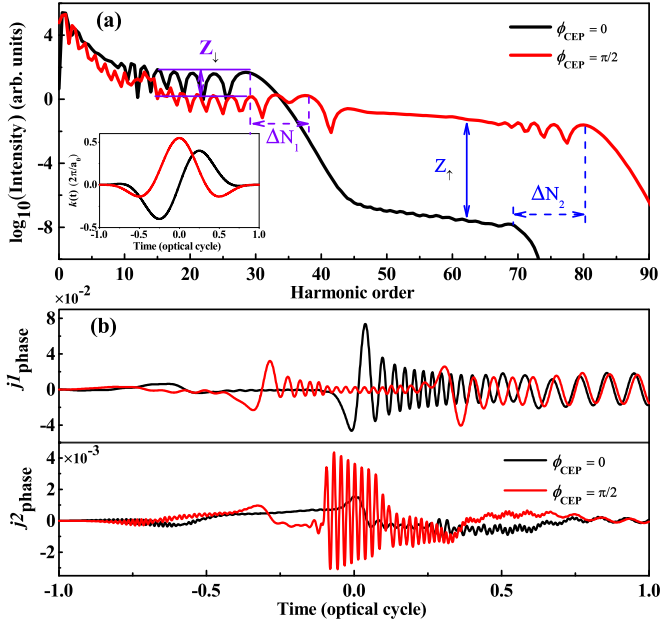


FIG. 4. The CEP effect on HHG spectra under the alternative picture. (a) The HHG spectra obtained with two CEPs. The inset shows the time-dependent wave vector  $k(t)$  with different CEPs. The intensity change and cutoff extension of the HHG spectra are marked with  $Z_{\downarrow}$  ( $Z_{\uparrow}$ ) and  $\Delta N_1$  ( $\Delta N_2$ ), respectively. Panel (b) shows the currents ( $j1_{\text{phase}}$  and  $j2_{\text{phase}}$ ), which contribute to the HHG spectra of the first and second plateaus, respectively. The intensity, wavelength, and duration of the driving laser pulses are  $0.56 \text{ TW/cm}^2$ ,  $3.2 \mu\text{m}$ , and two optical cycles, respectively. The chirp parameter  $\beta$  is zero.

and experimentally [14–16] recently. The spatial dependence of the enhanced laser electric field can be described approximately as (similar to Taylor expansion)

$$E(x, t) \approx E(t)(1 + \gamma x), \quad (11)$$

where  $\gamma$  has dimensions of inverse length (in unit of inverse of Bohr radius in atomic units) [39]. In experiments, the spatial nonhomogeneity factor  $\gamma$  can be changed by adjusting the shape of bow-tie nanostructures and the distance between two elements [16].

We show the harmonic spectra in the case of the homogeneous and nonhomogeneous fields with a nonhomogeneity parameter  $\gamma = 0.0004 \text{ a.u.}$  in Fig. 3(a). The double-plateau structure of the harmonic spectra is shown in both the homogeneous and nonhomogeneous fields. However, the second HHG plateau exhibits yield enhancement by two to three orders under the nonhomogeneous fields. The mechanisms of the yield enhancement had been previously interpreted with the populations and transition probabilities enhancement of the high-lying conduction bands [37]. Here, we turn to the alternative insight on the picture of the currents of  $j_{\text{phase}}$  and  $j_{\text{group}}$ . Figure 3(b) shows the distinction of the contributions in the HHG spectrum under the nonhomogeneous fields. One can observe that the contribution of  $j_{\text{phase}}$  dominates the double-plateau region. It implies that the main contribution of the HHG plateau has no changes between nonhomogeneous and homogeneous fields by comparing with the results in Fig. 2(b). A further insight is required to explain the only yield

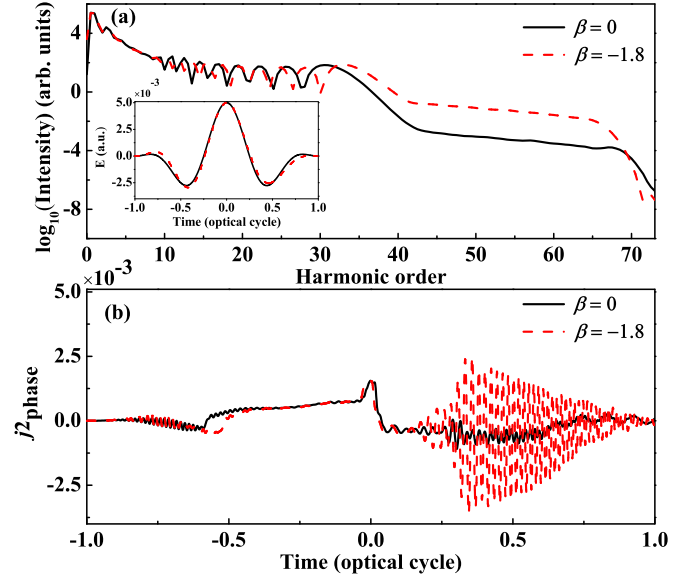


FIG. 5. Laser chirp effect on HHG spectra. (a) Comparison of the HHG spectra with different chirp parameters. The inset shows the laser pulses with different chirps. (b) The nonlinear currents  $j2_{\text{phase}}$  with different chirps, which give rise to the high-harmonic radiation of the second plateau. The intensity and wavelength of the laser pulses are the same as those in Fig. 2 except that the duration is two cycles.

enhancement of the second HHG plateau by focusing on the current  $j_{\text{phase}}$ . We divide the current  $j_{\text{phase}}$  into  $j1_{\text{phase}}$  and  $j2_{\text{phase}}$  by projection to the eigenstates of the first ( $C_1$ ) and high-lying ( $C_2$  plus  $C_3$ ) conduction bands, respectively, as shown in Fig. 3(c). The top of Fig. 3(c) illustrates that the  $j1_{\text{phase}}$  has the same magnitude in the case of homogeneous and nonhomogeneous fields, which explains why the change of the yield enhancement of the first plateau is not obvious. However, in the bottom of the Fig. 3(c), one can clearly see that the current  $j2_{\text{phase}}$  has a dramatic increment at the center of the laser pulses, which could give rise to two to three orders of yield enhancement of the second HHG plateau. The increment of the current  $j2_{\text{phase}}$  suggests that the intensity of the electronic polarization between each two atomic sites is enhanced in the case of nonhomogeneous fields, which leads to the enhancement of the second plateau high-order harmonic radiation.

Then, we focus on the effects of CEP and chirps [38,40] on the HHG spectra presented in Figs. 4 and 5. The form of the laser fields is expressed as

$$E(t) = E_0 f(t) \cos[\omega t + \phi_{\text{CEP}} + \phi(t)], \quad (12)$$

where  $\phi(t) = \beta(\frac{t}{\tau})^2$ , and  $\beta$  is a chirp parameter.  $\tau$  is fixed to 610 a.u.  $\phi_{\text{CEP}}$  represents the CEP phase.  $\omega$  and  $f(t)$  are the frequency and  $\cos^2$  envelope function of the laser fields respectively.

The cutoff extensions of the two plateaus are obvious and marked with  $\Delta N_1$  and  $\Delta N_2$  in Fig. 4(a). Due to the bigger wave vector  $k$  in the laser pulses with  $\phi_{\text{CEP}} = \pi/2$ , as shown in the inset of Fig. 4(a), the cutoff extensions can be clarified easily based on the previous quasiclassical analysis of the dynamics [24]. One can also find that the intensity of double-plateau HHG changes dramatically in the case of the laser pulses with different CEPs. The second HHG plateau has a magnitude

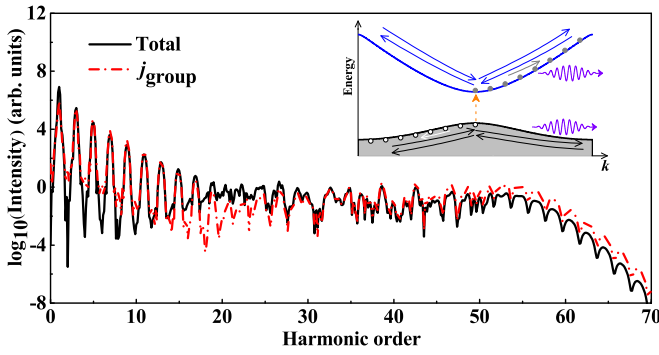


FIG. 6. HHG spectrum in the THz fields with a central frequency of 18.7 THz and an intensity of  $3.16 \text{ GW/cm}^2$ . The parameter  $V_0$  is 0.2 a.u. in the periodic potential. The inset shows the mechanisms of the HHG in the THz fields.

enhancement of six to seven orders ( $Z_\uparrow$ ), however, the yield of the first HHG plateau decreases by one to two orders ( $Z_\downarrow$ ) in the case of the fields with  $\phi_{\text{CEP}} = \pi/2$ . To clarify the mechanisms of this phenomenon, we adopted the model mentioned above by distinguishing the currents  $j_{1\text{phase}}$  and  $j_{2\text{phase}}$  from the dominated contribution current  $j_{\text{phase}}$ , as illustrated in Fig. 4(b). The amplitude of the current  $j_{1\text{phase}}$  shows a small decrement in the fields with  $\phi_{\text{CEP}} = \pi/2$ , which leads to one to two orders intensity decrement of the first plateau. However, the  $j_{2\text{phase}}$  is enhanced obviously at the center of the laser pulses in the case of  $\phi_{\text{CEP}} = \pi/2$ , which gives rise to six to seven orders intensity enhancement of the second plateau.

We also investigate the laser chirp effect on the high-order harmonic emission, as shown in Fig. 5. Figure 5(a) shows an intensity enhancement phenomenon of the second HHG plateau, which can also be attributed to the enhancement of the nonlinear current  $j_{2\text{phase}}$  with a chirp parameter  $\beta = -1.8$  in Fig. 5(b). One could conclude that the effects of CEP and chirp regulate the electron polarizations between neighboring lattice sites, which leads to the yield decrease or enhancement of the HHG plateau.

Finally, we investigate the mechanisms of the HHG process in the THz fields [9,29,41], as presented in Fig. 6. One can find that the dominant contribution of the HHG spectrum originates from the current  $j_{\text{group}}$  [29], which implies that the Bloch wave packet oscillates back and forth in the coordinate space with a group velocity under the THz fields. The instantaneous oscillation between two lattice sites can be neglected in the THz fields. As a result, the current  $j_{\text{phase}}$  caused by the electronic polarization between two neighboring atomic sites can be ignored. Consequently, the mechanisms of the HHG in the THz fields differentiate from those in the midinfrared laser fields. It is in agreement with recent experimental measurements in Ref. [41]. The picture can be comprehended in the  $k$  space, as shown in the inset of Fig. 6. A THz driver field induces weak photoionization (vertical orange arrow), pumping electrons to conduction bands, creating holes in valence band, and driving the electron and hole wave-packet dynamics in the conduction

and valence bands. The electron and hole oscillate separately back and forth (shown by blue and black arrows), giving rise to the emission of the high-order harmonics. It reveals that the dominant mode of the wave-packet oscillation determines the mechanisms of the HHG in the laser fields, which range from midinfrared to THz fields.

#### IV. SUMMARY

In summary, this work reveals an alternative model on the HHG from solids by focusing on the dynamics of the Bloch wave packet, which moves at group and phase velocities in coordinate space. The physical picture of this model shows a good correspondence to the model in momentum space with intra- and interband dynamic processes. It is a universal way to deal with the chirp, CEP, and nonhomogeneous laser fields. It is valid ranging from midinfrared to THz fields. It provides an instructive scheme for experimental measurements to determine the mechanisms of the HHG by distinguishing the dynamic modes of the wave packets.

#### ACKNOWLEDGMENTS

The authors thank Hui-Hui Yang and Cheng Gong very much for valuable discussions. This work is supported by the National Natural Science Foundation of China (Grants No. 21501055, No. 11404376, No. 11561121002 and No. 11674363).

#### APPENDIX

In this Appendix, we show the details of the derivation of Eq. (10) from Eq. (9) [34]. The envelope function  $\Phi(x,t)$  is defined by

$$\begin{aligned} \Phi(x,t) &= \int_{-\frac{\Delta k}{2}}^{\frac{\Delta k}{2}} e^{i[\delta k \cdot (x - \frac{[\nabla_k \epsilon_n(k)]_{k_0} t}{\hbar})]} d(\delta k) \\ &\approx \frac{\sin \frac{\Delta k}{2} \zeta}{\frac{\Delta k}{2} \zeta}, \end{aligned} \quad (\text{A1})$$

where  $\zeta = x - \frac{1}{\hbar} (\frac{\partial \epsilon_n(k)}{\partial k})_{k_0} t$ . The initial wave function is a Bloch eigenstate when  $t = 0$ , so the  $\Delta k \rightarrow 0$  and the envelope  $|\Phi(x,t)| = 1$ , as shown in the bottom panels of Fig. 1.  $\Delta k$  is not equal to 0 under the laser fields, so the amplitude of the envelope function has a maximum only when the parameter  $\zeta = 0$ . If we define the central position of the time-dependent wave packet as the coordinate of the Bloch electron, it can be written as

$$x = \frac{1}{\hbar} \left( \frac{\partial \epsilon_n(k)}{\partial k} \right)_{k_0} t. \quad (\text{A2})$$

The group velocity of the Bloch electron can be written as

$$v_g(k) = \dot{x} = \frac{1}{\hbar} \frac{\partial \epsilon_n(k)}{\partial k} \Big|_k. \quad (\text{A3})$$

[1] T. Brabec and F. Krausz, *Rev. Mod. Phys.* **72**, 545 (2000).

[2] F. Krausz and M. Ivanov, *Rev. Mod. Phys.* **81**, 163 (2009).

[3] S. Ghimire, A. D. DiChiara, E. Sistrunk, P. Agostini, L. F. DiMauro, and D. A. Reis, *Nat. Phys.* **7**, 138 (2011).

- [4] G. Vampa, T. J. Hammond, N. Thiré, B. E. Schmidt, F. Légaré, C. R. McDonald, T. Brabec, and P. B. Corkum, *Nature (London)* **522**, 462 (2015).
- [5] K. F. Lee, X. Ding, T. J. Hammond, M. E. Fermann, G. Vampa, and P. B. Corkum, *Opt. Lett.* **42**, 1113 (2017).
- [6] T. Higuchi, M. I. Stockman, and P. Hommelhoff, *Phys. Rev. Lett.* **113**, 213901 (2014).
- [7] G. Vampa and T. Brabec, *J. Phys. B* **50**, 083001 (2017).
- [8] G. Ndabashimiye, S. Ghimire, M. Wu, D. A. Browne, K. J. Schafer, M. B. Gaarde, and D. A. Reis, *Nature (London)* **534**, 520 (2016).
- [9] O. Schubert, M. Hohenleutner, F. Langer, B. Urbanek, C. Lange, U. Huttner, D. Golde, T. Meier, M. Kira, S. W. Koch, and R. Huber, *Nat. Photon.* **8**, 119 (2014).
- [10] M. Hohenleutner, F. Langer, O. Schubert, M. Knorr, U. Huttner, S. W. Koch, M. Kira, and R. Huber, *Nature (London)* **523**, 572 (2015).
- [11] Y. S. You, D. A. Reis, and S. Ghimire, *Nat. Phys.* **13**, 345 (2016).
- [12] H. Liu *et al.*, *Nat. Phys.* **13**, 262 (2016).
- [13] T. Tamaya, A. Ishikawa, T. Ogawa, and K. Tanaka, *Phys. Rev. Lett.* **116**, 016601 (2016).
- [14] G. Vampa, B. G. Ghamsari, S. S. Mousavi, T. J. Hammond, A. Olivieri, E. L. Skrek, A. Y. Naumov, D. M. Villeneuve, A. Staudte, P. Berini, and P. B. Corkum, *Nat. Phys.* **13**, 659 (2017).
- [15] J. D. Cox, A. Marini, and F. J. G. D. Abajo, *Nat. Commun.* **8**, 14380 (2016).
- [16] S. Han, H. Kim, Y. W. Kim, Y.-J. Kim, S. Kim, I.-Y. Park, and S.-W. Kim, *Nat. Commun.* **7**, 13105 (2016).
- [17] C. Liu, Y. Zheng, Z. Zeng, and R. Li, *Phys. Rev. A* **93**, 043806 (2016).
- [18] C. Yu, X. Zhang, S. Jiang, X. Cao, G. Yuan, T. Wu, L. Bai, and R. Lu, *Phys. Rev. A* **94**, 013846 (2016).
- [19] X. Liu, X. Zhu, P. Lan, X. Zhang, D. Wang, Q. Zhang, and P. Lu, *Phys. Rev. A* **95**, 063419 (2017).
- [20] L.-N. Li and F. He, *J. Opt. Soc. Am. B* **34**, 52 (2017).
- [21] G. Vampa, C. R. McDonald, G. Orlando, P. B. Corkum, and T. Brabec, *Phys. Rev. B* **91**, 064302 (2015).
- [22] K. J. Schafer, B. Yang, L. F. DiMauro, and K. C. Kulander, *Phys. Rev. Lett.* **70**, 1599 (1993).
- [23] P. B. Corkum, *Phys. Rev. Lett.* **71**, 1994 (1993).
- [24] T.-Y. Du and X. B. Bian, *Opt. Express* **25**, 151 (2017).
- [25] G. R. Jia, X. H. Huang, and X. B. Bian, *Opt. Express* **25**, 23654 (2017).
- [26] P. G. Hawkins and M. Y. Ivanov, *Phys. Rev. A* **87**, 063842 (2013).
- [27] S. Ghimire, A. D. DiChiara, E. Sistrunk, G. Ndabashimiye, U. B. Szafruga, A. Mohammad, P. Agostini, L. F. DiMauro, and D. A. Reis, *Phys. Rev. A* **85**, 043836 (2012).
- [28] C. R. McDonald, G. Vampa, P. B. Corkum, and T. Brabec, *Phys. Rev. A* **92**, 033845 (2015).
- [29] M. Garg, M. Zhan, T. T. Luu, H. Lakhotia, T. Klostermann, A. Guggenmos, and E. Goulielmakis, *Nature (London)* **538**, 359 (2016).
- [30] D. Golde, T. Meier, and S. W. Koch, *Phys. Rev. B* **77**, 075330 (2008).
- [31] S. Glutsch, *Phys. Rev. B* **69**, 235317 (2004).
- [32] M. S. Wismer, S. Y. Kruchinin, M. Ciappina, M. I. Stockman, and V. S. Yakovlev, *Phys. Rev. Lett.* **116**, 197401 (2016).
- [33] M. Wu, S. Ghimire, D. A. Reis, K. J. Schafer, and M. B. Gaarde, *Phys. Rev. A* **91**, 043839 (2015).
- [34] K. Huang, *Solid State Physics* (Higher Education Press, Beijing, China, 1988).
- [35] J. M. Ziman, *Principles of the Theory of Solids* (Cambridge University Press, Cambridge, England, 1972).
- [36] J. C. Slater, *Phys. Rev.* **87**, 807 (1952).
- [37] T. Y. Du, Z. Guan, X. X. Zhou, and X. B. Bian, *Phys. Rev. A* **94**, 023419 (2016).
- [38] Z. Guan, X. X. Zhou, and X. B. Bian, *Phys. Rev. A* **93**, 033852 (2016).
- [39] M. F. Ciappina, J. Biegert, R. Quidant, and M. Lewenstein, *Phys. Rev. A* **85**, 033828 (2012).
- [40] T. T. Luu, M. Garg, S. Yu. Kruchinin, A. Moulet, M. Th. Hassan, and E. Goulielmakis, *Nature (London)* **521**, 498 (2015).
- [41] F. Langer, M. Hohenleutner, C. P. Schmid, C. Poellmann, P. Nagler, T. Korn, C. Schüller, M. S. Sherwin, U. Huttner, J. T. Steiner, S. W. Koch, M. Kira, and R. Huber, *Nature (London)* **533**, 225 (2016).